Research Article

Facile Synthesis of N-Doped BiOCl Photocatalyst by an Ethylenediamine-Assisted Hydrothermal Method

Guihua Chen,[1,2] Gangling Chen,[1] Yong Wang,[1,2] Qingfeng Wang,[1] and Zhen Zhang[3]

[1]*School of Pharmaceutical and Chemical Engineering, Taizhou University, Jiaojiang 318000, China*
[2]*Jiangsu Key Laboratory for Environment Functional Materials, Suzhou University of Science and Technology, Suzhou 215009, China*
[3]*School of Bioscience, Taizhou University, Taizhou, Jiaojiang 318000, China*

Correspondence should be addressed to Yong Wang; wangyong@tzc.edu.cn

A nitrogen doped BiOCl (N-BiOCl) photocatalyst was synthesized and characterized using an ethylenediamine-assisted hydrothermal method. The N-BiOCl sample demonstrated the same tetragonal crystal structure as the as-prepared pure BiOCl sample. SEM results indicated that N-BiOCl sample was self-assembled by nanoplates to provide an aggregated flower-like microstructure. Doped nitrogen was substituted for oxygen in the crystal lattice of BiOCl, causing a red shift for N-BiOCl sample compared to BiOCl sample. The N-BiOCl sample exhibited higher photocatalytic activity in the degradation of Rhodamine B under visible light than observed in BiOCl sample, and the stability of the sample was verified. Meanwhile, speculative causes for the enhancement in the photocatalytic activity of N-BiOCl sample were also proposed.

1. Introduction

Photocatalysis is regarded as a promising application technology in the fields of air cleaning and water purification [1]. Over the years, many semiconductor materials have been exploited for photocatalysis. As an important kind of V-VI-VII main group ternary semiconductors, bismuth oxide haloids (BiOXs, X = Cl, Br, I) have a layered structure consisting of alternately arranged $[Bi_2O_2]^{2+}$ mono layers and dual X^- layers [2]. This layered structure facilitates the separation of photogenerated electron-hole pairs; therefore BiOXs could show excellent photocatalytic activity [3]. For example, Zhang et al. [4] have found better performance of BiOCl in the photocatalytic degradation of methyl orange as compared to the standard TiO_2 (P25, Degussa). However, BiOCl absorbs only UV light and is theoretical inability to degrade organic contaminants under visible light due to its wide band gap. As a result, widespread efforts have been dedicated to the exploration of functional BiOCl-based visible light photocatalysts by incorporating metal ions or coupling with other semiconductors [5].

In a pioneering study by Asahi et al. [6], nitrogen doped TiO_2 (N-TiO_2) was utilized to narrow the band gap of TiO_2 for the attainment of photocatalytic activity under visible light. While the use of nitrogen doping is still under debate, the concept of nitrogen doping has been successfully employed to reduce the band gap for other types of photocatalysts [7], such as ZnO [8], $SrTiO_3$ [9], and $Sr_2Ta_2O_7$ [10]. Inspired by the success of N-TiO_2 endowed with photocatalytic activity under visible light, it is feasible to apply the nitrogen doping on BiOCl to make BiOCl visible light active.

Herein, N-BiOCl sample was synthesized by an ethylenediamine-assisted hydrothermal method. Its photocatalytic activity was evaluated under visible light for the degradation of Rhodamine B (RhB) solution and compared to the pure BiOCl sample.

2. Experimental

All chemicals were of analytical grade and were used as received without purification. A typical synthesis procedure of N-BiOCl sample was followed, in which 2 mmol of

$Bi(NO_3)_3 \cdot 5H_2O$ was dissolved in 20 mL of 1 mol/L HNO_3 to form a clear solution, and 2 mmol of KCl was dissolved in 30 mL of deionized water. Both solutions were then mixed with stirring, and a white precipitate was quickly formed. The pH of the suspension was subsequently adjusted to 7 through the addition of ethylenediamine (EDA). After continuous stirring for 60 min, the homogeneous mixture was transferred into a 100 mL Teflon container. Afterwards, the container was subjected to hydrothermal treatment at 160°C for 20 h and then cooled to room temperature. The resulting precipitate was filtered, successively washed with deionized water, and finally dried at 60°C in a vacuum oven. The pure BiOCl sample was prepared through a similar method just using 1 mol/L of NaOH aqueous solution to adjust the pH to 7.

X-ray diffraction (XRD) patterns were recorded on D8 Advance diffractometer using Cu Kα radiation. UV-vis diffuse reflectance spectroscopy (DRS) was obtained on U-4100 spectrometer. The morphology of the samples was examined using an S-4800 scanning electron microscopy (SEM) with an accelerating voltage of 15 kV. The specific surface area (S_{BET}) and pore size distribution (PSD) of the samples were measured from N_2 adsorption-desorption isotherms at −196°C with a Micromeritics ASAP-2020 analyzer after the samples were degassed in a vacuum at 120°C for 3 h. X-ray photoelectron spectroscopy (XPS) using an Al Kα radiation source with 1486.6 eV energy was performed on a PHI 550 Philips to investigate the surface properties.

The photocatalytic degradation of RhB over the samples was carried out in a XPA-II photocatalytic reactor (Nanjing Xujiang Electromechanical Factory). A 500 W Xe lamp, mainly emitting visible light in the range of 400–800 nm, was used as the light source and placed in a quartz socket tube with one end closed. Water was circulated through the interlayer to cool the system and magnetic stirring was used to suspend the photocatalyst in the reaction solution.

The suspension consisted of 100 mL 10 mg/L RhB and 0.1 mg sample. Prior to visible light irradiation, the suspension was stirred under the condition of 1 mL/min airflow for 30 min to establish an adsorption-desorption equilibrium between the sample surfaces and RhB. During the entire degradation process, the stirring was maintained in the suspension under the same airflow condition. At regular irradiation intervals, 5 mL of the suspension was extracted using a syringe. The RhB concentration was analyzed by a UV-vis spectrophotometer (Shimadzu, UV-2450), and the absorbance wavelength was determined at 553 nm.

3. Results and Discussion

Figure 1 shows the XRD patterns of BiOCl and N-BiOCl samples. All of the diffraction peaks are precisely indexed to the characteristic Bragg diffraction of tetragonal crystal structure of BiOCl (JCPDS number 06-0249) [11] in the as-synthesized samples. Interestingly, a trace of Bi_2O_3 diffraction peak is observed in BiOCl sample, while this was not detected in N-BiOCl sample. It was presumably attributed to stronger alkalinity in NaOH than in EDA.
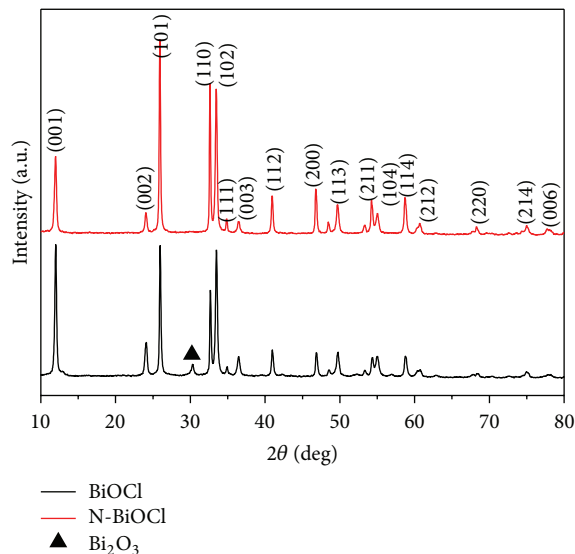

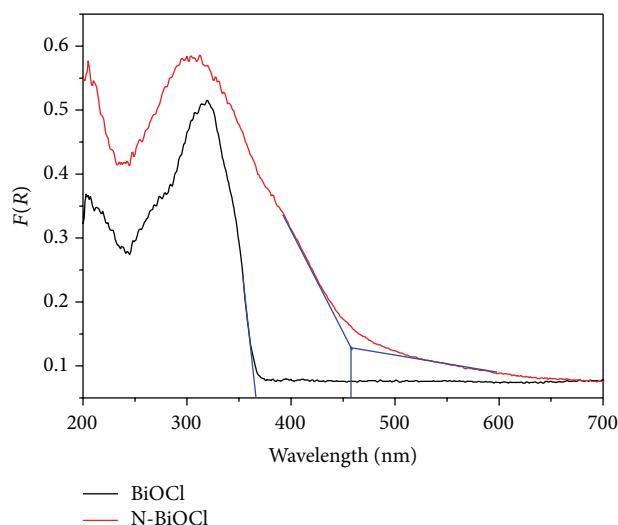FIGURE 1: XRD patterns of BiOCl and N-BiOCl samples.

FIGURE 2: DRS spectra of BiOCl and N-BiOCl samples.

Figure 2 displays the UV-vis diffuse reflectance spectra of BiOCl and N-BiOCl samples. The onset of band gap absorption in BiOCl sample is determined at 367 nm, whereas the absorption edge of N-BiOCl sample demonstrates an obvious red shift to a longer wavelength. This could be attributed to the effect of nitrogen doping, which results in an extended photoresponse region for BiOCl. It was also supposed that the N-BiOCl sample was more effective in absorbing visible light, promoting the degradation of RhB under visible light.

Figure 3 reveals the SEM images of BiOCl and N-BiOCl samples. The BiOCl sample is of close-packed nanoplates (Figure 3(a)) with irregular shape (Figure 3(c)), and the surfaces of the nanoplates are smooth (Figure 3(b)). The morphology of N-BiOCl sample is shown at various magnification levels (Figures 3(d)–3(f)). In contrast with BiOCl

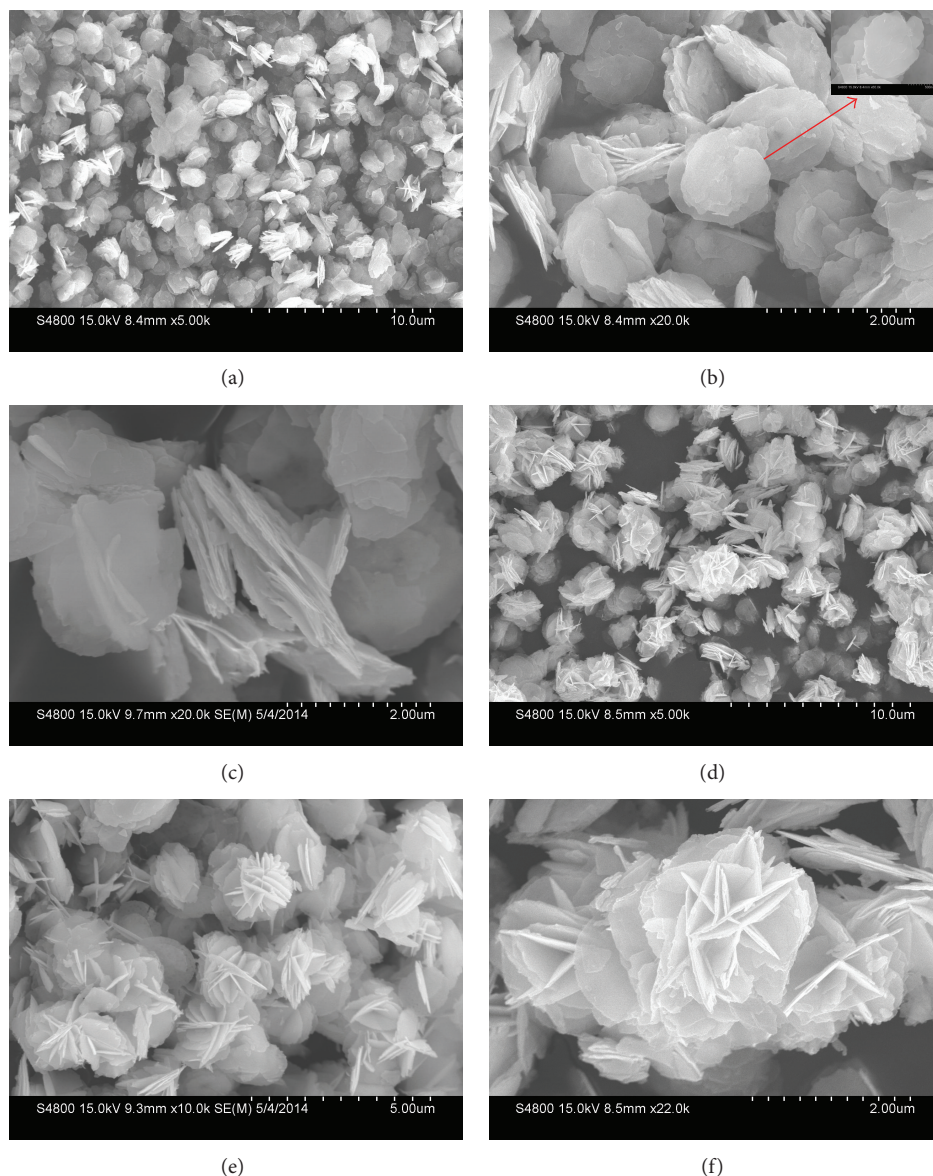(a)

(b)

(c)

(d)

(e)

(f)

Figure 3: SEM micrographs of BiOCl (a, b, and c) and N-BiOCl (d, e, and f) samples.

sample, N-BiOCl sample is comprised of numerous self-assembled loose nanoplates, forming large quantities of flower-like microstructures. Based on the aforementioned data, EDA was established as a significantly influential factor for the overall morphology of the final product. The exact mechanism of this formation is currently under investigation and the results will be presented in due course.

XPS is illustrated for BiOCl and N-BiOCl samples in Figure 4. The survey spectra (Figure 4(a)) confirm the presence of Bi, O, Cl, and C elements in BiOCl sample. The peak for C 1s was ascribed to the adventitious carbon from the XPS instrument. Aside from the anticipated similarities in peaks, a singular peak (marked with blue circle) is identified in N-BiOCl sample. As displayed in Figure 4(b), the peak located at 400.3 eV is assigned to N 1s [8], indicating that nitrogen atoms were inserted into BiOCl during the hydrothermal process.

The band gap of BiOCl sample was modified and narrowed due to the substitution of nitrogen for oxygen atoms in the lattice of BiOCl, and the atomic concentration of doped nitrogen was determined to be 1.2% by XPS.

Figure 5(a) shows nitrogen adsorption-desorption isotherms of BiOCl and N-BiOCl sample. In accordance with IUPAC classification, the isotherms are categorized as type-IV with a H3 hysteresis loop, implying the presence of a mesoporous region. These results are further confirmed by the corresponding PSD curves (Figure 5(b)), which are bimodal with smaller and larger mesopores in the BiOCl and N-BiOCl samples. As the nanoplates did not contain pores (inset of Figure 3(b)), the smaller mesopores could be derived from porosity within the nanoplates. The larger mesopores could be ascribed to the pores formed between the stacked or intercrossed nanoplates, as indicated by the
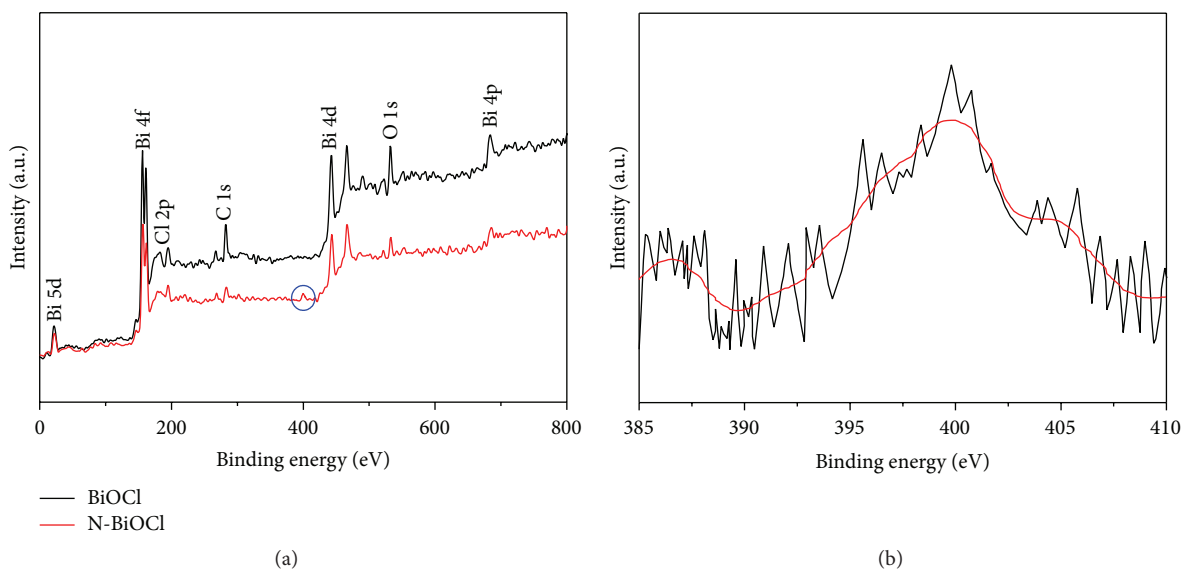
FIGURE 4: XPS spectra of BiOCl and N-BiOCl samples for survey (a) and N 1s (b).
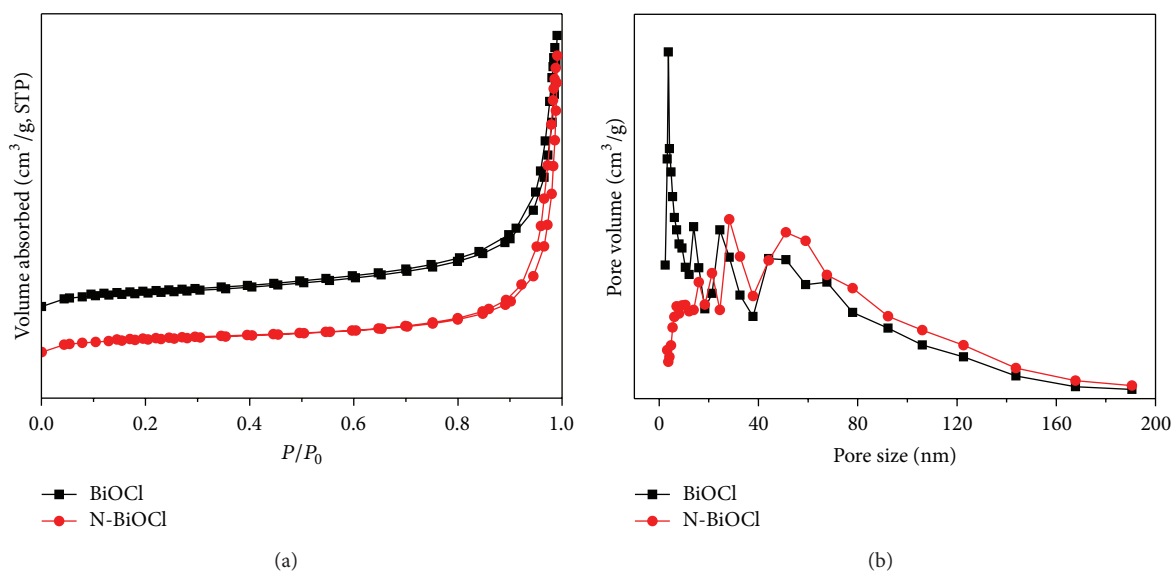

FIGURE 5: N$_2$ adsorption-desorption isotherms (a) and pore size distribution curves (b) of BiOCl and N-BiOCl samples.

SEM micrographs. The S_{BET} values of the BiOCl and N-BiOCl samples calculated from N$_2$ adsorption isotherms are 8.54 and 6.09 m^2/g, respectively.

Although the adsorptive ability of BiOCl sample was slightly superior to that of N-BiOCl sample, the N-BiOCl sample exhibited higher photocatalytic activity than BiOCl sample for the degradation of RhB under visible light (**Figure 6**). The causes for the enhanced photocatalytic activity in N-BiOCl sample were discussed as follows. Nitrogen doping might be helpful for absorption of visible light by elevating the valence band maximum to narrow the band gap with N 1s states or forming some localized N 1s states in the band gap [12]. In addition, the N-BiOCl sample was

favorable in retaining the multiple scattering of light within the self-assembled flower-like framework, leading to more effective light harvesting [13]. Thus, the degradation rate of RhB solution for N-BiOCl sample was accelerated under visible light.

For the purpose of investigating the stability of N-BiOCl sample, five cycles of experiment were carried out in the same conditions. After each complete period of photocatalytic reaction, aqueous solution containing the sample was centrifuged and supernatant was emptied. It was found that the photocatalytic performance did not have a sharp decline, indicating that N-BiOCl sample did not suffer the instability (**Figure 7**). The trace quantities of the sample with
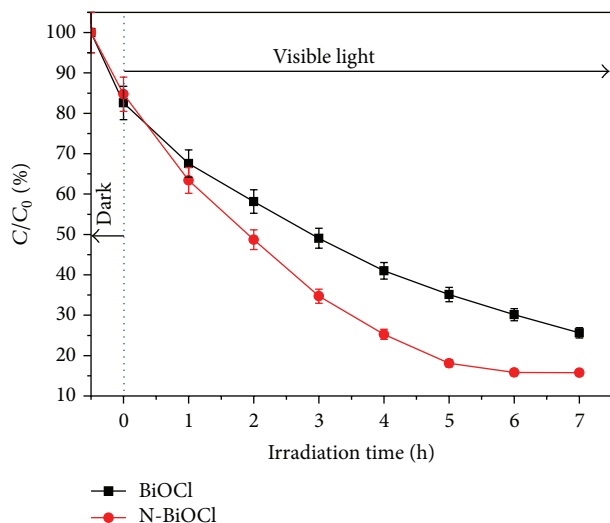
FIGURE 6: The photocatalytic activity of BiOCl and N-BiOCl samples under visible light (C_0: original concentration of RhB, C: instant concentration of RhB at irradiation time).
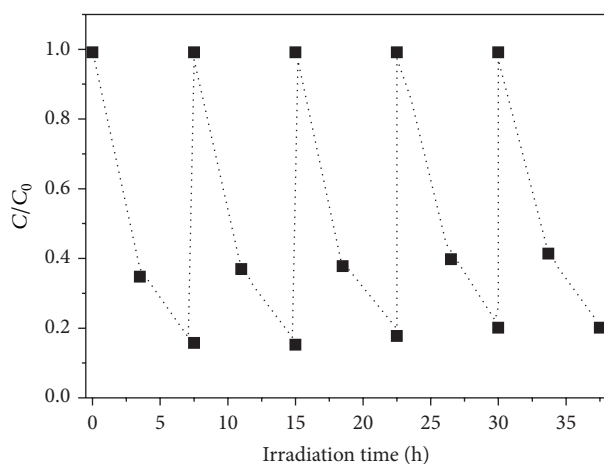

FIGURE 7: Stability and cycles of N-BiOCl sample in the degradation of RhB.

supernatant are poured off, which cause the decrease of degradation rate of RhB.

4. Conclusions

In summary, an ethylenediamine-assisted hydrothermal method has been developed for the synthesis of N-BiOCl sample. Nitrogen doping influenced the morphology and optical absorption range of pure BiOCl sample, resulting in improved photocatalytic activity for the decomposition of RhB under visible light as compared with BiOCl sample. In addition, N-BiOCl sample still showed a significant capacity for RhB degradation after five cycles of reuse.

Conflict of Interests

The authors declare that there is no conflict of interests regarding the publication of this paper.

References

[1] P. Y. Dong, Y. H. Wang, B. C. Cao et al., "Ag_3PO_4/reduced graphite oxide sheets nanocomposites with highly enhanced visible light photocatalytic activity and stability," *Applied Catalysis B: Environmental*, vol. 132-133, pp. 45–53, 2013.

[2] N. Kijima, K. Matano, M. Saito et al., "Oxidative catalytic cracking of *n*-butane to lower alkenes over layered BiOCl catalyst," *Applied Catalysis A: General*, vol. 206, no. 2, pp. 237–244, 2001.

[3] Y. Ao, H. Tang, P. Wang, C. Wang, J. Hou, and J. Qian, "Synthesis, characterization and photocatalytic activity of BiOBr-AC composite photocatalyst," *Composites Part B: Engineering*, vol. 59, pp. 96–100, 2014.

[4] K. L. Zhang, C. M. Liu, F. Q. Huang, C. Zheng, and W. D. Wang, "Study of the electronic structure and photocatalytic activity of the BiOCl photocatalyst," *Applied Catalysis B: Environmental*, vol. 68, no. 3-4, pp. 125–129, 2006.

[5] Q. Z. Wang, J. Hui, Y. J. Huang et al., "The preparation of BiOCl photocatalyst and its performance of photodegradation on dyes," *Materials Science in Semiconductor Processing*, vol. 17, pp. 87–93, 2014.

[6] R. Asahi, T. Morikawa, T. Ohwaki, K. Aoki, and Y. Taga, "Visible-light photocatalysis in nitrogen-doped titanium oxides," *Science*, vol. 293, no. 5528, pp. 269–271, 2001.

[7] F. Dong, H. T. Liu, W.-K. Ho, M. Fu, and Z. B. Wu, "$(NH_4)_2CO_3$ mediated hydrothermal synthesis of N-doped $(BiO)_2CO_3$ hollow nanoplates microspheres as high-performance and durable visible light photocatalyst for air cleaning," *Chemical Engineering Journal*, vol. 214, pp. 198–207, 2013.

[8] H. Bai, Z. Liu, and D. D. Sun, "Hierarchical nitrogen-doped flowerlike ZnO nanostructure and its multifunctional environmental applications," *Chemistry*, vol. 7, no. 8, pp. 1772–1780, 2012.

[9] F. Zou, Z. Jiang, X. Q. Qin et al., "Template-free synthesis of mesoporous N-doped $SrTiO_3$ perovskite with high visible-light-driven photocatalytic activity," *Chemical Communications*, vol. 48, no. 68, pp. 8514–8516, 2012.

[10] A. Mukherji, B. Seger, G. Q. Lu, and L. Wang, "Nitrogen doped $Sr_2Ta_2O_7$ coupled with graphene sheets as photocatalysts for increased photocatalytic hydrogen production," *ACS Nano*, vol. 5, no. 5, pp. 3483–3492, 2011.

[11] J. H. Yu, B. Wei, L. Zhu, H. Gao, W. J. Sun, and L. L. Xu, "Flowerlike C-doped BiOCl nanostructures: facile wet chemical fabrication and enhanced UV photocatalytic properties," *Applied Surface Science*, vol. 284, pp. 497–502, 2013.

[12] G. Q. Zhu, J. Liang, M. Hojamberdiev et al., "Ethylenediamine (EDA)—assisted hydrothermal synthesis of nitrogen-doped Bi_2WO_6 powders," *Materials Letters*, vol. 122, pp. 216–219, 2014.

[13] W. X. Guo, F. Zhang, C. J. Lin, and Z. L. Wang, "Direct growth of TiO_2 nanosheet arrays on carbon fibers for highly efficient photocatalytic degradation of methyl orange," *Advanced Materials*, vol. 24, no. 35, pp. 4761–4764, 2012.